Supporting Information for

Naphthodithiophene Diimide-Based Copolymers: Ambipolar Semiconductors in Field Effect Transistors and Electron Acceptors with Near-Infrared Response in Polymer Blend Solar Cells

Kyohei Nakano[1‡], Masahiro Nakano[1‡], Bo Xiao[2], Erjun Zhou[2,*], Kaori Suzuki[1], Itaru Osaka[1], Kazuo Takimiya[1,*], and Keisuke Tajima[1,3,*]

[1]RIKEN Center for Emergent Matter Science (CEMS), 2-1 Hirosawa, Wako, Saitama 351-0198, Japan,

[2]CAS Key Laboratory of Nanosystem and Hierarchical Fabrication, CAS Center for Excellence in Nanoscience, National Center for Nanoscience and Technology, Beijing 100190, P. R. China.

[3]Precursory Research for Embryonic Science and Technology (PRESTO), Japan Science and Technology Agency, 4-1-8 Honcho, Kawaguchi, Saitama 332-0012, Japan

[‡] *These two authors contributed equally to this work.*

Electronic mail: keisuke.tajima@riken.jp; takimiya@riken.jp; zhouej@nanoctr.cn

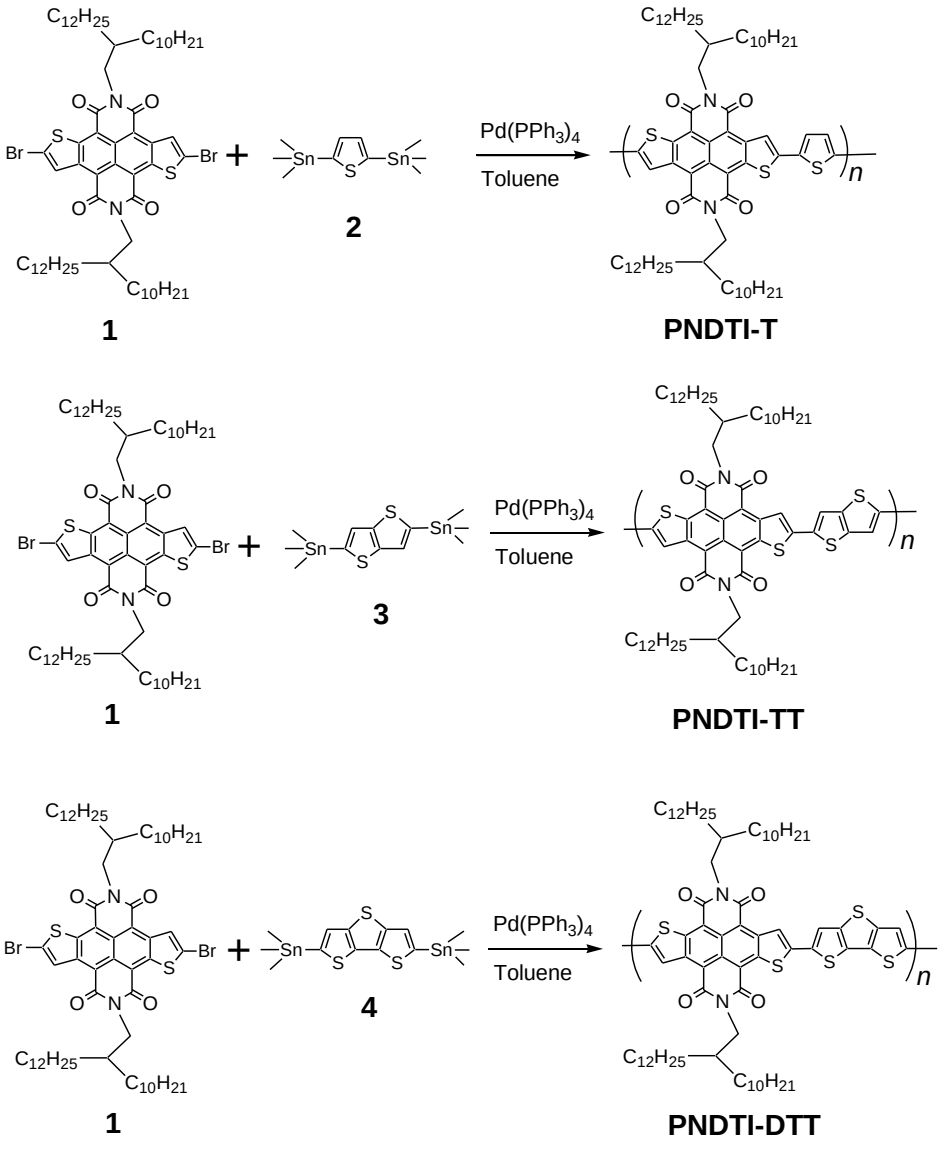

Scheme S1. Chemical structures and synthetic routes for PNDTI-T, PNDTI-TT, and PNDTI-DTT.

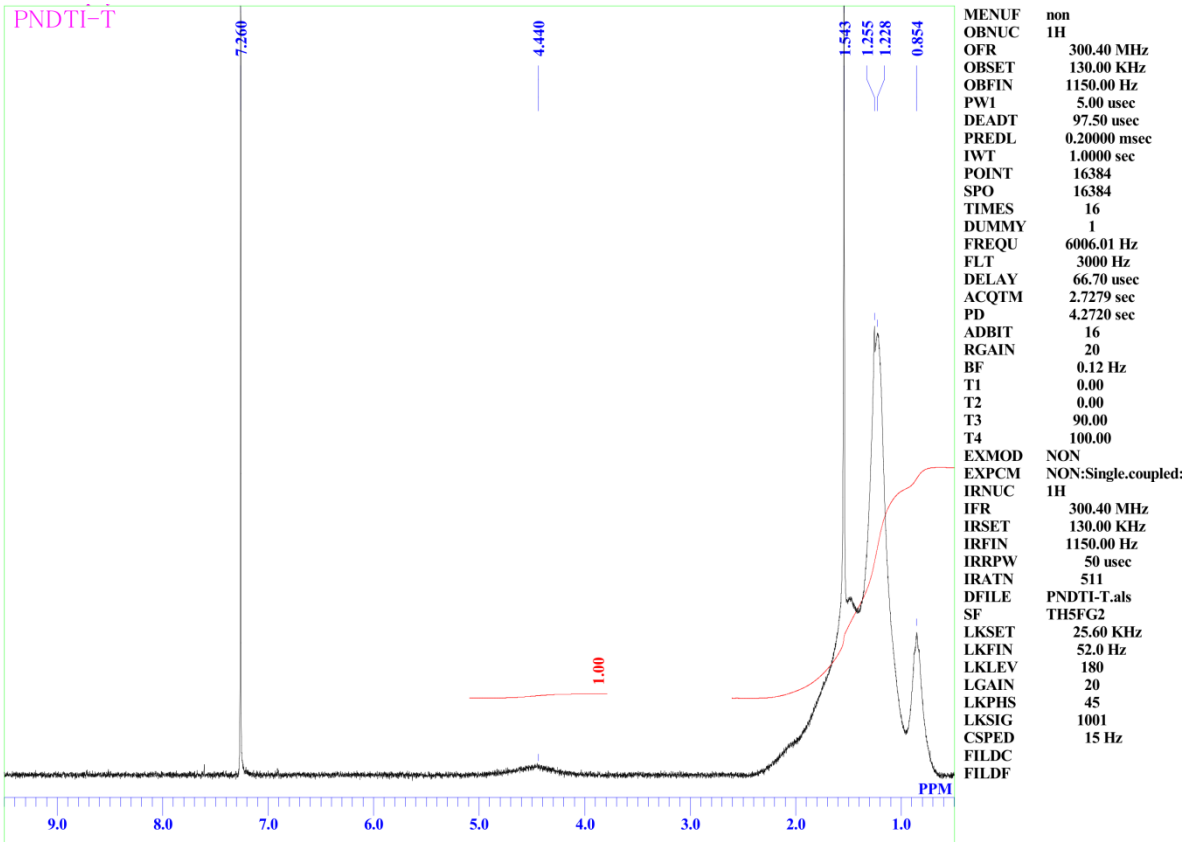

Figure S1. ^{1}H NMR chart of PNDTI-T in $CDCl_3$.

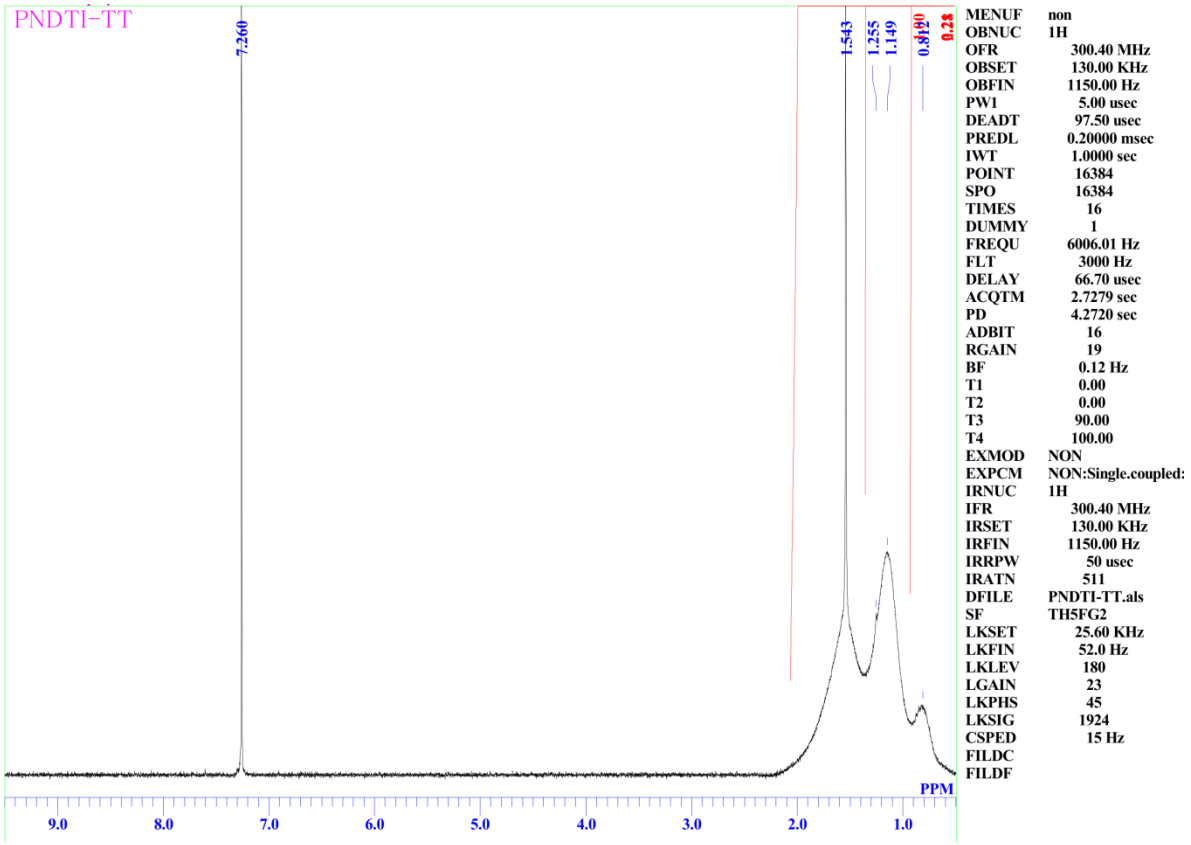

Figure S2. ^{1}H NMR chart of PNDTI-TT in $CDCl_3$.

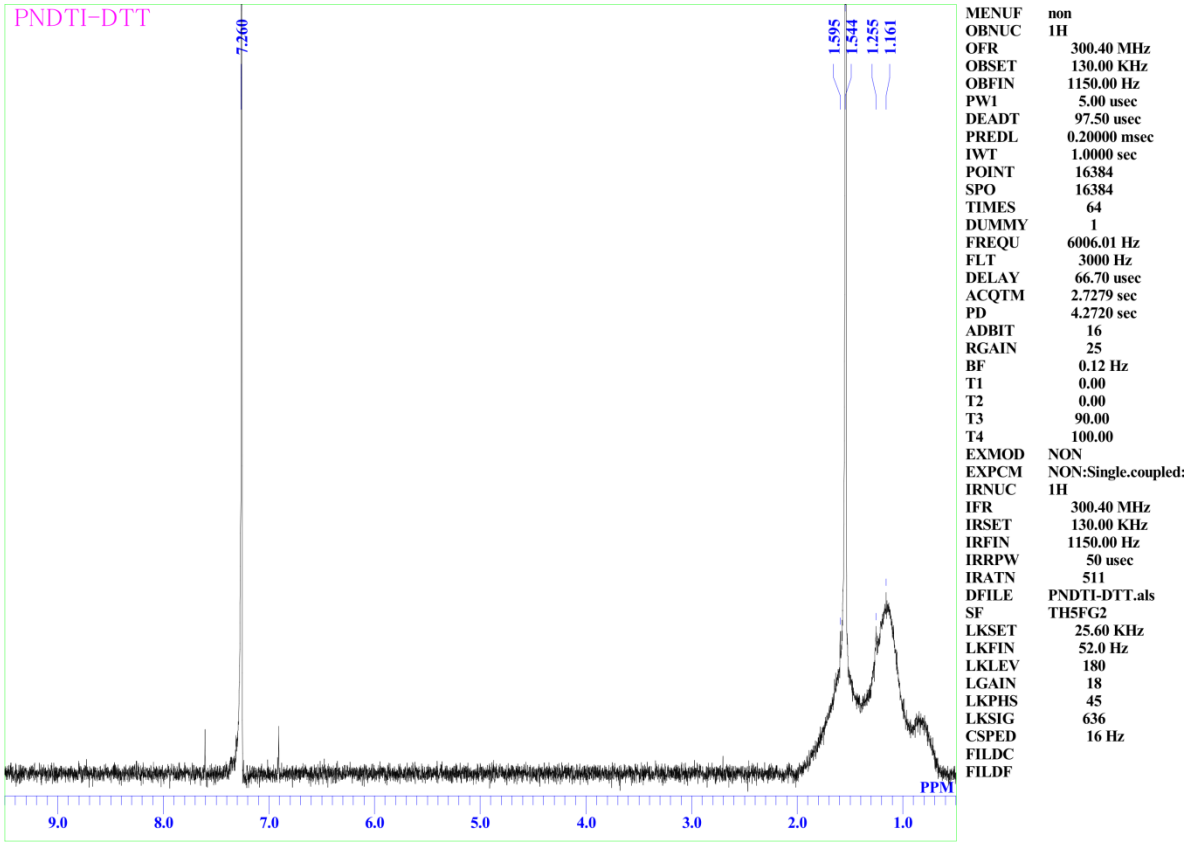

Figure S3. ^{1}H NMR chart of PNDTI-DTT in $CDCl_3$.

Table S1. Reduction and oxidation potentials of PNDTIs vs Ag/AgCl determined by cyclic voltammetry.

	E_{red} (eV)	E_{ox} (eV)
PNDTI-T	−0.29	1.48
PNDTI-TT	−0.28	1.38
PNDTI-DTT	−0.32	1.27

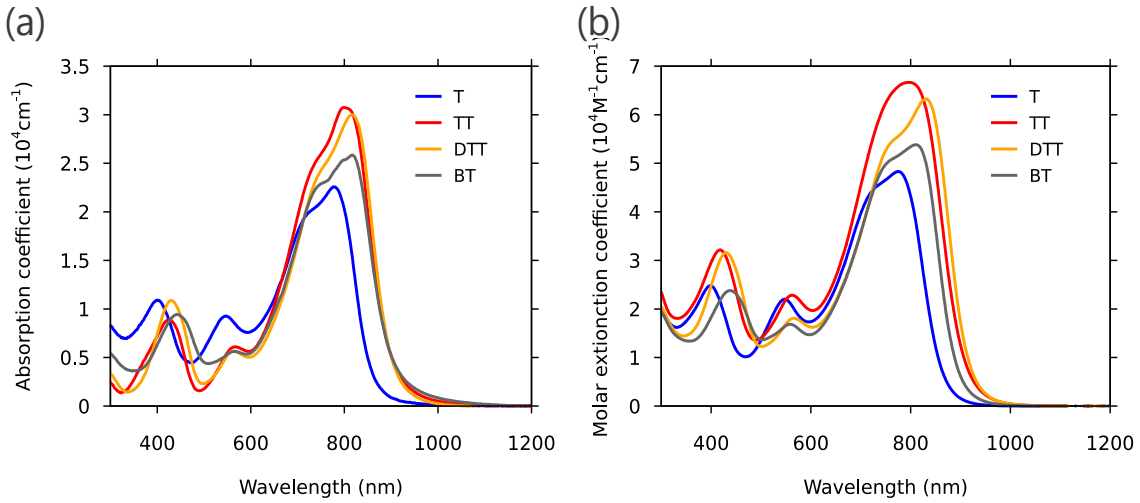

Figure S4. (a) Absorption coefficient of PNDTI thin films and (b) molar extinction coefficient of PNDTI in chlorobenzene solution.

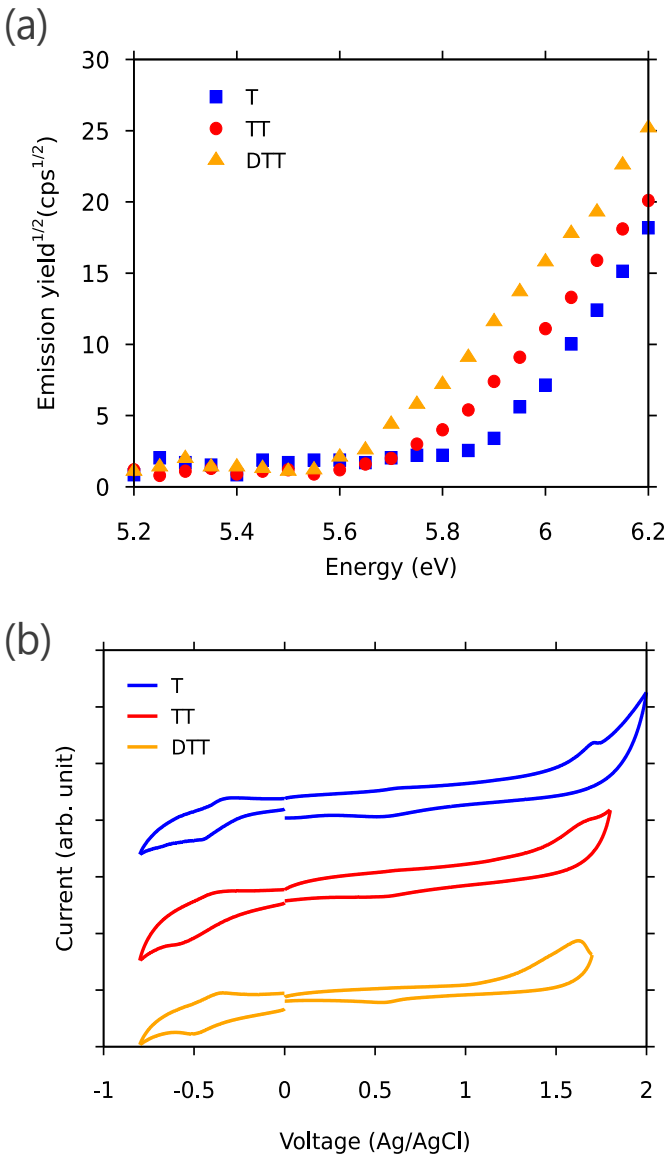

Figure S5. (a) Photoelectron spectra in air (AC-2, Riken Keiki) and (b) cyclic voltammograms for PNDTIs.

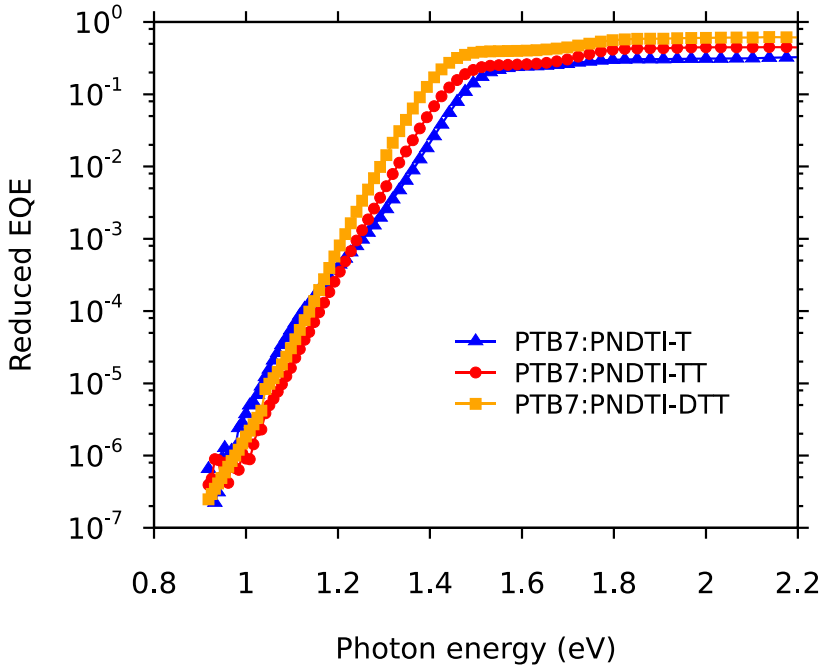

Figure S6. External quantum efficiency of PTB7:PNDTIs BHJ cells as a function of irradiated photon energy obtained with the high-sensitivity lock-in technique.

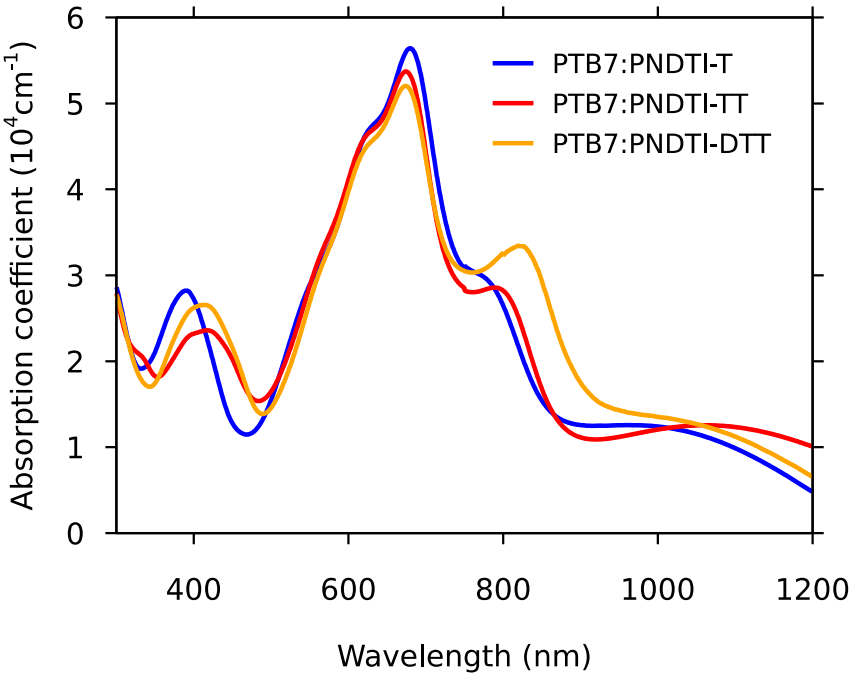

Figure S7. Absorption coefficient of BHJ thin films of PTB7:PNDTIs.

Table S2. Summary of device performance with various film thicknesses. All films were thermally annealed at 80 °C for 30 min in an N_2-filled glovebox.

	PTB7:PNDTI-T			**PTB7:PNDTI-TT**			**PTB7:PNDTI-DTT**		
Thickness (nm)	172	144	121	160	120	100	162	121	100
V_{OC} **(V)**	0.55	0.57	0.56	0.61	0.61	0.62	0.65	0.66	0.66
J_{SC} **(mA/cm^2)**	3.4	4.8	4.8	4.9	5.8	6.4	9.3	9.8	9.6
FF	0.42	0.43	0.46	0.42	0.45	0.50	0.47	0.50	0.51
PCE (%)	0.78	1.2	1.2	1.2	1.6	2.0	2.8	3.2	3.2

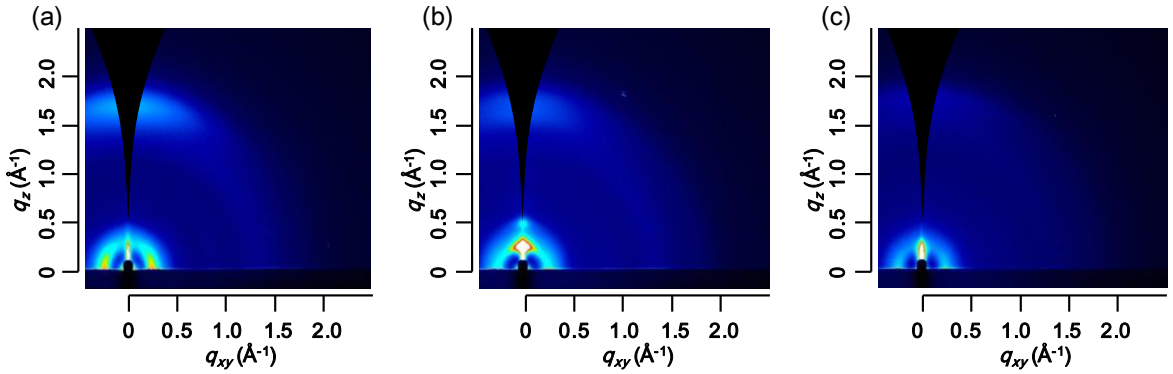

Figure S8. 2D Grazing incident angle X-ray diffraction patterns of PTB7:PNDTI thin films. (a) PTB7:PNDTI-T, (b) PTB7:PNDTI-TT, and (c) PTB7:PNDTI-DTT. As-cast films were used for the measurements.

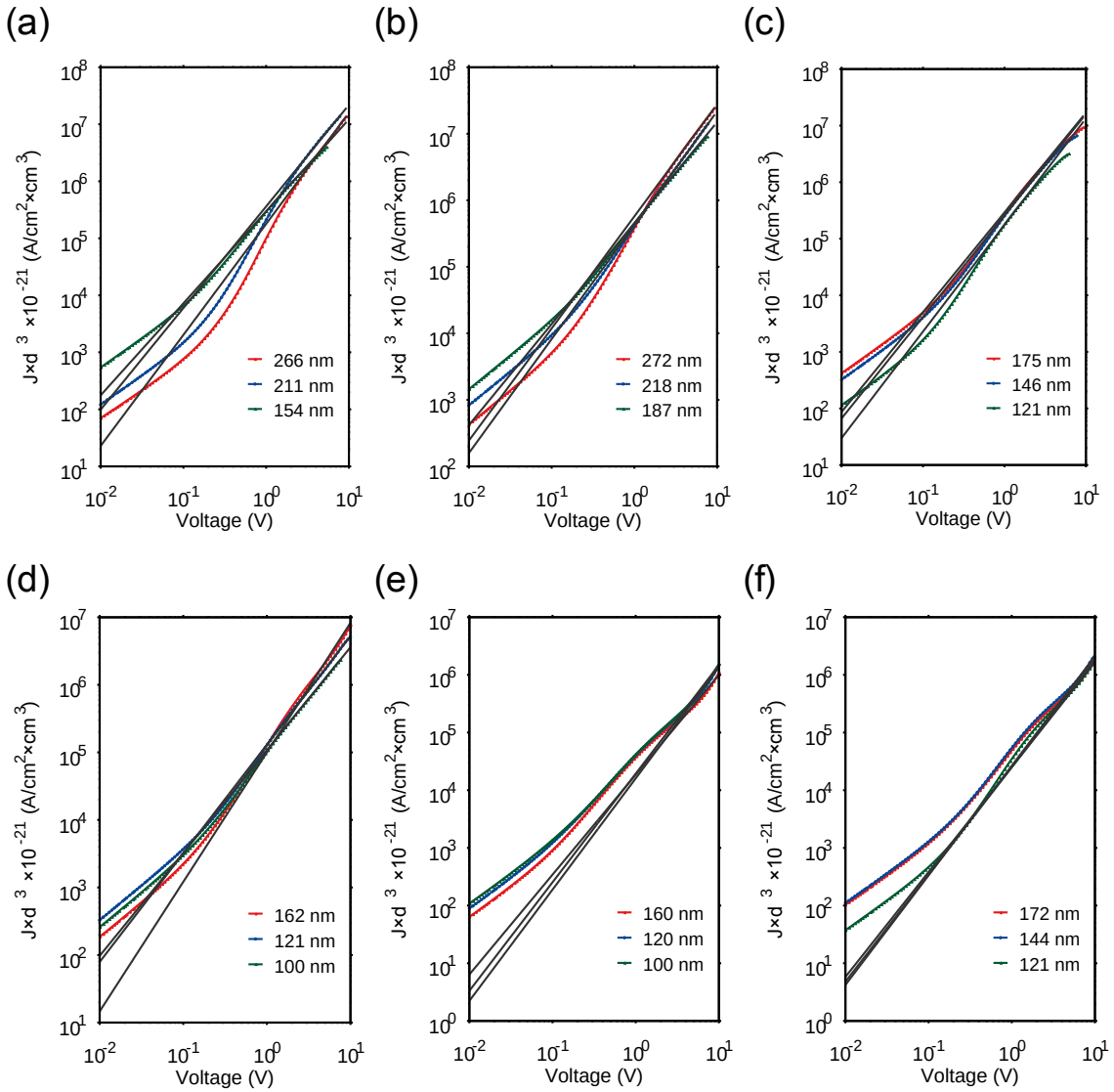

Figure S9. Current density normalized by the cube of the film thickness (*d*) plotted against voltage for the electron-only devices with the pristine films of (a) PNDTI-T, (b) PNDTI-TT, and (c) PNDTI-DTT and for the mixed films of (d) PTB7:PNDTI-T, (e) PTB7:PNDTI-TT, and (f) PTB7:PBDTI-DTT.

Table S3. Summary of the average slope of *J*-*V* curves used for analyzing the Mott-Gurney law, and the average electron mobility in SCLC region with standard deviations in parentheses.

	PNDTI-T		PNDTI-TT		PNDTI-DTT	
Average values	Slope	μ_e (cm^2/V s)	Slope	μ_e (cm^2/V s)	Slope	μ_e (cm^2/V s)
Pristine thin film	1.83	$7.6(1.7) \times 10^{-4}$	1.76	$1.4(0.04) \times 10^{-3}$	1.83	$9.3(3.1) \times 10^{-4}$
Mixture with PTB7	1.86	$8.5(0.3) \times 10^{-5}$	1.85	$6.0(0.6) \times 10^{-5}$	1.62	$4.3(0.7) \times 10^{-4}$

Table S4. Summary of the device performance for PTB7:PNDTI-DTT with different annealing conditions and concentrations of diiodooctane (DIO) additive.

	PTB7:PNDTI-DTT						
Spin rate	3000	3000[a)]	3000	3000	3000	3000	3000
Addition of DIO (vol %)	0	0	0	0	1	3	5
Annealing (°C)	No	No	80	120	80	80	80
V_{OC} (V)	0.67	0.67	0.67	0.67	0.67	0.67	0.66
J_{SC} (mA/cm^2)	10.6	10.7	10.2	9.92	8.11	6.75	6.86
FF	0.50	0.50	0.50	0.50	0.47	0.50	0.50
PCE (%)	3.55	3.58	3.42	3.30	2.53	2.25	2.25

[a)]Using the inverted device structure of ITO/ZnO/active layer/MoO_x/Ag.